Anisotropic-Isotropic Transition of Cages at the Glass Transition

Huijun Zhang,[1,*] Qi Zhang,[2] Feng Liu,[1] and Yilong Han[2,3,†]
[1]State Key Laboratory for Mechanical Behavior of Materials, Shaanxi International Research Center for Soft Matter, School of Materials Science and Engineering, Xi'an Jiaotong University, 710049, Xi'an, China
[2]Department of Physics, Hong Kong University of Science and Technology, Clear Water Bay, Hong Kong
[3]Shenzhen Research Institute, The Hong Kong University of Science and Technology, Shenzhen, China

(Received 4 May 2023; revised 3 September 2023; accepted 12 January 2024; published 13 February 2024)

Characterizing the local structural evolution is an essential step in understanding the nature of glass transition. In this work, we probe the evolution of Voronoi cell geometry in simple glass models by simulations and colloid experiments, and find that the individual particle cages deform anisotropically in supercooled liquid and isotropically in glass. We introduce an anisotropy parameter k for each Voronoi cell, whose mean value exhibits a sharp change at the mode-coupling glass transition ϕ_c. Moreover, a power law of packing fraction $\phi \propto q_1^d$ is discovered in the supercooled liquid regime with $d > D$, in contrast to $d = D$ in the glass regime, where q_1 is the first peak position of structure factor, and D is the space dimension. This power law is qualitatively explained by the change of k. The active motions in supercooled liquid are spatially correlated with long axes rather than short axes of Voronoi cells. In addition, the dynamic slowing down approaching the glass transition can be well characterized through a modified free-volume model based on k. These findings reveal that the structural parameter k is effective in identifying the structure-dynamics correlations and the glass transition in these systems.

DOI: 10.1103/PhysRevLett.132.078201

Introduction.—Glasses or amorphous solids are produced by cooling [1] or densifying [2] liquids. As the glass transition is approached, dynamics slows down drastically without any noticeable structural change [3,4]. The mode-coupling theory (MCT) [5,6] or Vogel-Fulcher-Tamman (VFT) law [1] predicts the drastic growth of relaxation time τ_α before the glass transition but does not provide structural features. Although experiments [7–12] and simulations [13–20] have made intensive efforts in searching for effective structural parameters in characterizing the glass transition, the structural mechanism remains unclear. Whether glass transition has a structural origin or is purely dynamic remains controversial [1,21].

Great efforts have been devoted to identifying nonagnostic locally favored structures responsible for the dynamic slowing down. For instance, icosahedral [21,22], crystalline [9,12], and tetrahedral clusters [19,23] have been found to correlate with the slow dynamics in different glass-forming liquids, but these structural signatures are system dependent [24] and cannot distinguish glass structure from liquid because these motifs similarly exist in both liquid and glass regimes. In addition, structural indicators of icosahedra or tetrahedra [19,21–23] are not applicable for 2D systems. Since the explicit structure correlated with glassy dynamics is unknown, various indirect structural parameters, such as two-point entropy [9,25], soft spot from vibration modes [26], and neighboring structures from machine learning [27,28], have been proposed to link local structures with dynamic slowing down. However, these parameters do not have a simple geometrical meaning, i.e., structural agnostic, and do not exhibit a sharp change at the glass transition point. Recently, Ref. [17] proposed a relatively simple structural parameter about each particle's deviation from its reference structure, which correlates with dynamics in two- and three-dimensional systems and exhibits a change at the VFT glass transition [29]. Here, we propose another general and simple structure parameter that correlates with dynamics and exhibits a change at the MCT glass transition, and verify it by simulations and colloid experiments.

Another topic in glass studies is the structural power law [30,31]. For a D-dimensional crystal, its mean atomic volume must satisfy the power law, $v_a \propto a^D \propto q_1^{-D} \propto \phi^{-1}$, where a is the lattice constant. q_1 is the first peak position of the structure factor $S(q)$, and ϕ is the packing fraction. Amorphous solids also follow the power law [30]:

$$q_1 \propto \phi^{1/d}. \tag{1}$$

However, $d \neq D$ in many glasses [30–36], which gives rise to controversies on its mechanism. Recent studies showed that pressure (or equivalently, density) and composition changes lead to different power laws. Under pressure change (i.e., varying ϕ), $d = D$ in glasses for particles with the same softness, such as in binary Weeks-Chandler-Andersen (WCA) [37] and hard sphere (HS) glasses, but deviates from D when the system is composed of hard and soft particles [35]. Link q_1 in the reciprocal space to certain structural change in real space is difficult because $S(q_1)$ contains structures spanning broad length scales in real space. How the local deformations affect the power law in

 © 2024 American Physical Society

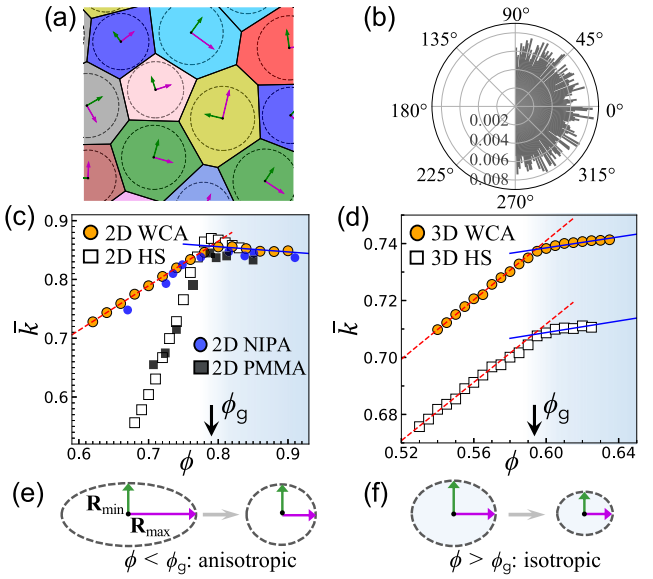

FIG. 1. Anisotropic-to-isotropic compression across the glass transition. (a) Radical Voronoi polygons of a subarea of the 2D WCA supercooled liquid at $\phi = 0.74$. The large eigenvector $\mathbf{R}_{max}$ (pink arrow) and small eigenvector $\mathbf{R}_{min}$ (green arrow) of the Voronoi polygons are labeled at the center of each particle (dashed circle). (b) The angular distribution of $\mathbf{R}_{max}$. $\mathbf{R}_{min}$ is always perpendicular to $\mathbf{R}_{max}$. (c) Average anisotropy $\bar{k}$ as a function of ϕ for 2D WCA (orange circles) and 2D HS (open squares) systems with size ratio $\lambda = 1.3$ and fraction of large particles $x = 0.5$. The supercooled liquid (red line) and glass (blue line) behaviors of 2D glasses intersect at $\phi_g \approx 0.79$. (d) Average anisotropy $\bar{k}$ as a function of ϕ for 3D WCA (orange circles) and 3D HS (open squares) systems with $\lambda = 1.3$ and $x = 0.5$. The supercooled liquid (red line) and glass (blue line) regimes for 3D systems intersect at $\phi_g \approx 0.59$. (e),(f) Schematic of the anisotropic deformation at $\phi < \phi_g$ and isotropic deformation at $\phi > \phi_g$, respectively.

reciprocal space remains unclear. Moreover, whether the power law holds in liquid regime and how it changes at the glass transition have not been explored.

Each particle in a supercooled liquid is caged by its nearest neighboring particles [38]. The cage effect has been widely used to qualitatively explain the dynamical behaviors [39,40] and plastic deformations [41,42]. However, a direct link between cage structure and glass transition remains unavailable. The cage of each particle is described by its Voronoi cell [43] [Fig. 1(a)], which reflects the particle's free volume not shared by its neighbors. Voronoi tessellation is usually applied to characterize the local packing of particles, which has been used to understand the jamming transition [44] and boson peak [45] in amorphous solids. Here, we find that the cage anisotropy can effectively reveal the structure change at the glass transition.

Methods.—We perform molecular dynamics simulations [46] for WCA particles and event-driven molecular dynamics simulations [47] for HSs in both 2D and 3D. Binary sized particles are used to avoid crystallization. The details of the simulation and colloid experiment are in the Supplemental Material [48].

Cage anisotropy parameter k.—We use radical Voronoi tessellation [43] [Fig. 1(a)] for binary systems to avoid the incorrect bisecting line cutting through a large sphere. The asymmetric shape of the Voronoi cell is characterized by a tensor [38,62], $\mathbf{I} = \int_V \mathbf{r} \otimes \mathbf{r} d\mathbf{r}$, which integrates over the cell volume V; $\mathbf{r}$ is the position vector relative to the particle's center and $\otimes$ denotes a dyadic product. $\mathbf{I}$ represents the shape of the Voronoi cell, and its principal axes are obtained by diagonalizing $\mathbf{I}$. The two orthogonal eigenvectors, $\mathbf{R}_{min}$ and $\mathbf{R}_{max}$, represent the short and long axes of the cage, respectively [Fig. 1(a)]. Their ratio defines the cage anisotropy parameter $k \equiv (|\mathbf{R}_{min}|/|\mathbf{R}_{max}|) \in (0, 1]$. $k = 1$ for an isotropic cage, and the deviation from 1 quantifies the elongation anisotropy of the cage. Similar parameters about the asymmetric elongation of the cage have been used to study soft colloidal glasses [38] and jamming transition in 3D HS systems [62]. However, the causal link between the anisotropy parameter and glass transition has rarely been explored. Figure 1(a) shows that $\mathbf{R}_{min}$ points to its neighboring particles, whereas $\mathbf{R}_{max}$ points to the gap between two neighbors. The uniform distribution of $\mathbf{R}_{max}$ directions in Fig. 1(b) manifests the random orientations of the cells.

Anisotropy and volume of cages at glass transition.—As ϕ increases, free volumes around particles are squeezed, yielding more isotropic cages, that is, higher averaged $\bar{k}$ [Figs. 1(c) and 1(d)]. In Fig. 1(c), $\bar{k}(\phi)$ increases and reaches a plateau at $\phi > 0.79$ for 2D WCA and 2D HS systems, demonstrating a structure change at their glass transitions. The increase in $\bar{k}(\phi)$ at $\phi < \phi_g$ in Fig. 1(c) shows that cages are compressed more along $\mathbf{R}_{max}$ than $\mathbf{R}_{min}$ direction as ϕ increases, that is, cage deformation is anisotropic, as illustrated in Fig. 1(e) and Supplemental Material Fig. S1 [48]. In the supercooled liquid regime, $\bar{k}$ is higher in 2D WCA than in 2D HS system [Fig. 1(c)] because the softer WCA particles can adjust their positions more easily to form more homogeneous structures with more isotropic cages. At $\phi > \phi_g$, $\bar{k}$ is comparable for 2D WCA and 2D HS systems because both WCA and HS particles interact via their hard cores at high ϕ. $\bar{k}$ is approximately constant at $\phi > \phi_g$ [Fig. 1(c)], indicating that cages isotropically deform in glasses [Fig. 1(f)]. Similar behavior of $\bar{k}$ is also observed in 3D WCA and 3D HS systems [Fig. 1(d)] and 2D WCA systems with different λ (Supplemental Material Fig. S2 [48]). $\bar{k}$ is lower in 3D systems than in 2D systems [Figs. 1(c) and 1(d)] because particles in the 3D system are more disordered and more difficult to adjust their positions due to stronger confinement from more neighboring particles. Alternatively, strong long-wavelength Mermin-Wagner

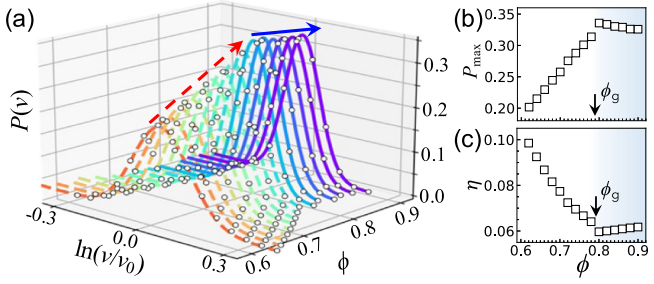

FIG. 2. Voronoi cell area v in 2D WCA systems. (a) Distributions of v fitted by the log-normal distribution (curves). $P(v)$ barely changes with ϕ at $\phi > 0.79$. Red and blue arrows show the increasing trend of the peaks in anisotropic ($\phi < 0.79$) and isotropic ($\phi > 0.79$) regimes, respectively. (b) The fitted maximum of $P(v)$. (c) The fitted standard deviation of $P(v)$.

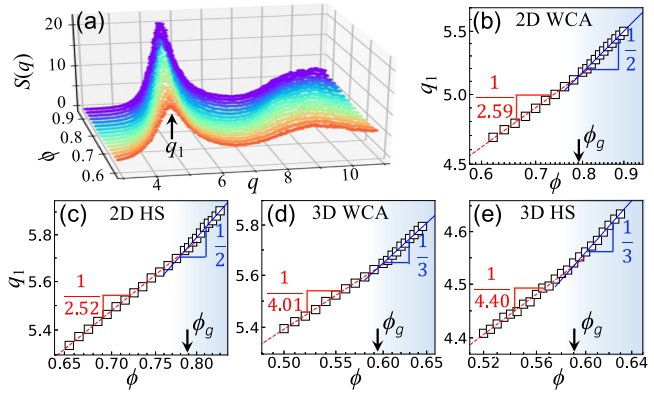

FIG. 3. Structural power law of Eq. (1). (a) $S(q)$ at $0.62 \le \phi \le 0.92$ for 2D WCA systems. (b)–(e) Log-log plots of $q_1(\phi)$ fitted with Eq. (1) (red and blue lines) for 2D WCA, 2D HS, 3D WCA, and 3D HS systems. The blue line with $d = D$ and the red line with $d > D$ intersect at ϕ_g. The values of $1/d$, that is, the slopes, are labeled in the figures.

fluctuations in 2D can better relax the structure [63], making ϕ_g high and HS and WCA glasses have similar degrees of disorder above such a high ϕ_g. By contrast, particles can easily jam at low ϕ in 3D due to the lack of Mermin-Wagner fluctuations [10,63], leading to a low ϕ_g. Consequently, the extremely high-ϕ glasses cannot be accessed and the soft WCA particles have not been compressed to HS-like in our accessible range of $\phi > \phi_g$ in 3D. Therefore, Voronoi cells of WCA particles are more isotropic (i.e., higher k) than those of HS particles in the whole range of ϕ because soft particles can better adjust their positions to reduce the cage anisotropy. We further confirm these expected structural disorders in 2D and 3D HS and WCA systems using the fluctuation of coordination number δz [Supplemental Material Figs. S3(c) and S3(d)], which shows similar behaviors to those in Figs. 1(c) and 1(d). These results demonstrate the effects of particle softness and space dimension on glass and supercooled liquid structures.

The results are experimentally tested using binary colloidal monolayers [48]. Figure 1(c) shows that the soft poly-N-isopropylacrylamide (NIPA) spheres [64] and hard poly(methyl methacrylate) (PMMA) [65] spheres behave similarly with the 2D WCA and 2D HS systems, respectively.

The anisotropic-to-isotropic transition of cage deformation [Figs. 1(c) and 1(d)] is further verified by the Voronoi cell volume v. Figure 2(a) shows that v of large particles satisfies a log-normal distribution well at each ϕ [66], $P(v) = (1/v\sqrt{2\pi}\eta)\exp\{-[(\ln v - \ln v_0)^2/2\eta^2]\}$. $P(v)$ barely changes at $\phi > 0.79$ in Fig. 2(a), implying isotropic shrinkages of cages, in accordance with Fig. 1(c). By contrast, the anisotropic deformations of cages at $\phi < 0.79$ change $P(v)$ in Fig. 2(a). The height and standard deviation of $P(v)$ exhibit a clear change at $\phi_g = 0.79$ [Figs. 2(b) and 2(c)], which is consistent with Fig. 1(c). $P(v)$ of small particles and 3D systems show similar transitions at ϕ_g (Supplemental Material Figs. S5 and S6 [48]).

Structural power law.—We generalize the power law Eq. (1) from glass [32,34,35] to supercooled liquid. q_1 in Eq. (1) is measured from the structure factor $S(q) = \langle \sum_{j=1}^{N} e^{i\mathbf{q}\cdot\mathbf{r}_j} \sum_{k=1}^{N} e^{-i\mathbf{q}\cdot\mathbf{r}_k} \rangle / N$. As ϕ increases, the interparticle distance decreases and q_1 increases [Fig. 3(a)]. For glasses composed of binary particles with the same softness, the compression is locally uniform, and thus $d = D$ [35]. Large and small spheres in 2D WCA systems have the same WCA potential, that is, the same softness, so the compression-induced deformation is spatially uniform [35]. Consequently, the exponent $d = D = 2$, which is confirmed in the glass regime at $\phi_g > 0.79$ [Fig. 3(b)]. The power law still holds in the supercooled liquid regime, however, $d = 2.59 > D$ for 2D WCA. Such $d = D$ in the glass regime and $d > D$ in the supercooled liquid regime have also been observed in 2D HS [Fig. 3(c)], 3D WCA [Fig. 3(d)], 3D HS [Fig. 3(e)], and 2D WCA systems at different λ and x (Supplemental Material Fig. S7 [48]). Thus, the coincidence between the glass transition and anisotropic-isotropic transition of cage deformation is robust.

d deviating from D has been observed in various metallic glasses under composition change [30,36] or glasses composed of particles with different softness under pressure change [32,35]. Such deviation manifests nonuniform deformations, but the type of deformation that can increase or decrease d is unclear [32,33]. Here, we find that $d > D$ in supercooled liquid [Figs. 3(b)–3(e)] arises from local anisotropic deformation [Fig. 1(e)]. d reflects the changing rate of ϕ and q_1 in a series of samples instead of certain structure in a single sample. For a global density change, the compressed volume Δv contributed from one anisotropic cage is equivalent to those from several isotropic cages because anisotropic cages usually have more free volumes than isotropic cages. Furthermore, a large Δv

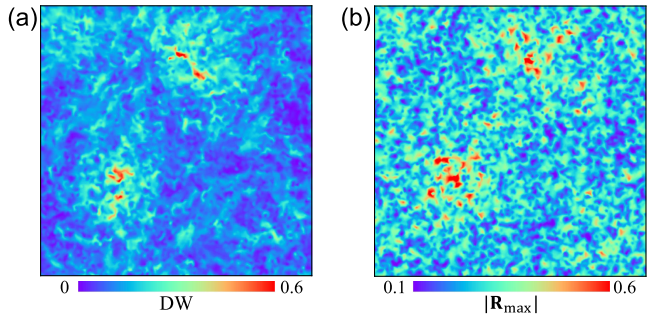

FIG. 4. Spatial correlation between dynamics (DW) and structure ($|\mathbf{R}_{max}|$) in the 2D WCA system at $\phi = 0.74$. (a) Spatial distribution of the DW factor. Red denotes strong dynamics. (b) Spatial distribution of $|\mathbf{R}_{max}|$.

concentrated at one place (i.e., one anisotropic cage) affects less on q_1 than multiple small Δv spread in the sample (i.e., multiple isotropic cages). Therefore, the same change in ϕ causes less change in q_1 for supercooled liquid because supercooled liquids contain more anisotropic cages. The slope of $q_1(\phi)$ is thereby lower in supercooled liquid, and the corresponding d is larger [Figs. 3(b)–3(e)]. Consequently, the transition between $d > D$ and $d = D$ [Figs. 3(b)–3(e)] corresponds to the anisotropic-isotropic transition of cages at the glass transition. Equation (1) arises from the structure change rather than the structure at a certain ϕ; thus, it is not related to any fractal structure in glass, and d can be greater than D [36].

Structure-dynamics correlations.—The dynamics of particle i is characterized by the Debye-Waller factor $\mathrm{DW}_i = \sqrt{\langle(\mathbf{r} - \langle\mathbf{r}\rangle)^2\rangle}/\bar{\sigma}$, where $\langle\rangle$ denotes the average over a time before cage breaking [67], and $\bar{\sigma}$ is the average particle diameter. Particles with large DW factors (i.e., strong dynamics) in Fig. 4(a) are spatially localized and more correlated with the large-$|\mathbf{R}_{max}|$ regions in Fig. 4(b), implying that particles tend to move along $\mathbf{R}_{max}$ rather than $\mathbf{R}_{min}$ (Supplemental Material Fig. S9 [48]). Therefore, $\mathbf{R}_{max}$ reflects a particle's dynamical propensity. This is reasonable because more free volume distributes along $\pm\mathbf{R}_{max}$ [Fig. 5(a)].

The structure relaxation time τ_α is measured as the decay time of the self-intermediate scattering function [Supplemental Material Fig. S15(a) [48]]. τ_α can be fitted by the MCT relation [1,5] $\tau_\alpha \sim (\phi_c - \phi)^{-\gamma}$ with $\phi_c = 0.785$ [Fig. 5(b)]. It coincides well with the structure transitions in Figs. 1(c), 2(b), 2(c), and 3(b), that is, $\phi_c = \phi_g$. Considering that $\bar{k}(\phi)$ is linear in the supercooled liquids [Fig. 1(c)], the MCT relation can be rewritten as

$$\tau_\alpha \sim (k_c - \bar{k})^{-\gamma}. \tag{2}$$

In contrast to the classic MCT relation based on the global thermodynamic parameter ϕ (or T), Eq. (2) links the glassy dynamics to specific local structure at the single-particle level in supercooled liquids. The fitted $k_c \approx 0.847$ [Fig. 5(c)] is consistent with the measured $\bar{k} = 0.85$ in the glass regime [Fig. 1(c)]. We attribute the increasing dynamic slowing down in supercooled liquids to the increase in $\bar{k}$, that is, cages becoming more isotropic [Fig. 1(f)], which reduces the free volume and mobility of particles.

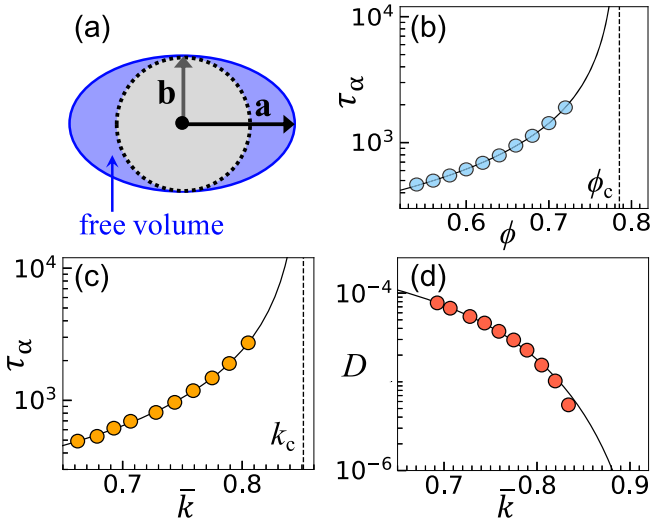

FIG. 5. Dynamical behavior of 2D WCA systems. (a) Schematic of the anisotropic cage (ellipse) composed of the particle (gray circle) and free volume (blue region). (b) Relaxation time $\tau_\alpha(\phi)$ with the MCT fit (curve) yields $\phi_c = 0.785$ and $\gamma = 1.07$. (c) $\tau_\alpha(\bar{k})$ fitted with Eq. (2) (curve) yields $k_c = 0.85$ and $\gamma = 0.97$. (d) Diffusion constant fitted with Eq. (3) (curve) where $A = 5 \times 10^{-4}$ and $B = 0.84$.

Free-volume model.—The free-volume mode is one of the most widely used and simplest theories for the glass transition [1,68,69], which attributes the dynamic slowing down to the decreased "free volume to move" for particles as ϕ increases [1]. If the free volume is known, then it can predict the average long-time diffusion constant of particles as $D(v_f) = A\exp(-B/v_f)$, where $v_f = (\bar{v} - v_0)/v_0$ is the reduced free volume, A is a temperature-dependent coefficient related to molecular diameter and velocity, and B is a factor in [0.5, 1] [68]. v_0 is the volume of a particle, and $\bar{v}$ is the specific volume [68]. However, this model does not consider the packing structure [68], and v_f is unavailable. Here, we suggest that v_f can be evaluated on the basis on k of the local cage. Considering that free volumes mainly locate along the long axis, the reduced free volume can be derived from our ellipse approximation of the cage, as shown in Fig. 5(a), $v_f = [(\pi \cdot |\mathbf{a}| \cdot |\mathbf{b}| - \pi \cdot |\mathbf{b}|^2)/(\pi \cdot |\mathbf{b}|^2)] = (1/k) - 1$ with $(\mathbf{R}_{min}/\mathbf{R}_{max}) = (\mathbf{b}/\mathbf{a})$, that is, the blue region in Fig. 5(a). This result is robust for 3D spheroid approximation: $v_f = [(\frac{4}{3}\pi \cdot |\mathbf{a}| \cdot |\mathbf{b}|^2 - \frac{4}{3}\pi \cdot |\mathbf{b}|^3)/(\frac{4}{3}\pi \cdot |\mathbf{b}|^3)] = (1/k) - 1$. Substituting v_f to $D(v_f)$ [68] gives

$$D(\bar{k}) = A\exp\left(\frac{-B\bar{k}}{1-\bar{k}}\right). \tag{3}$$

Equation (3) establishes a direct link between the diffusion and the geometric parameter k with free coefficients determined from the fitting.

The measured D satisfies Eq. (3) well in Fig. 5(d), indicating that the anisotropy parameter k can provide a single-particle form of the free-volume model. The cage-relative mean-square displacement (CRMSD) is defined as $\Delta r^2_{\mathrm{CR}}(t) = \langle[\tilde{\mathbf{r}}_i(t) - \tilde{\mathbf{r}}_i(0)]^2\rangle$ [10,70], where $\langle\rangle$ is the ensemble average. The long-time D is measured from the slope of the CRMSD at $t > 10^4$ [Supplemental Material Fig. S15(b) [48]].

Discussion.—In this Letter, we propose a structure parameter k with a simple geometrical meaning to characterize the cage anisotropy. $\bar{k}$ exhibits different behavior in supercooled liquid and glass regimes, and the structural anisotropic–isotropic transition coincides with the dynamic MCT glass transition at ϕ_c. This is robust in both 2D and 3D systems with isotropic interactions [Figs. 1(c) and 1(d) and Supplemental Material Fig. S2 [48]], providing a structural signature at the MCT glass transition point. A separate work is that we find that the structural power law also exists in the supercooled liquid regime, but its exponent $d > D$ in contrast to the power law in glasses [30–35] (Fig. 3).

Two applications of k are further studied. (1) The structural power laws in glass and supercooled liquids are qualitatively explained by the free-volume change associated with k. (2) Substituting k into the classical free-volume model yields Eq. (3), which can explain and predict the diffusion constant of D from the structure at the particle scale [Eq. (3) and Fig. 5(d)]. k reflects the local free volume. $\mathbf{R}_{\max}$ reflect a particle's dynamical propensity; that is, particles tend to move along $\pm\mathbf{R}_{\max}$ because more free volumes exist along this direction. Thus, k and $\mathbf{R}_{\max}$ can connect to mechanical behaviors of glass, such as soft spot [71,72] and shear transformation zone [73,74]. Moreover, we expect that k is also applicable in characterizing the crystallization [75–78] and melting transitions [79], in which the local cages will change from anisotropic in liquids to isotropic in crystals.

We thank Peng Tan and Hua Tong for helpful discussions. This work was supported by the National Natural Science Foundation of China (Grant No. 12274336), the Key R&D Project of Shaanxi Province (Grant No. 2022GY-400), the Fundamental Research Funds for Central Universities (Grant No. xxj032021001), Hong Kong Research Grants Council (Grants No. CRF-C6016-20G and No. C6021-19EF), and the Guangdong Basic and Applied Basic Research Foundation (Grant No. 2020B1515120067).

*huijun@xjtu.edu.cn
†yilong@ust.hk

[1] L. Berthier and G. Biroli, Rev. Mod. Phys. **83**, 587 (2011).
[2] G. Parisi and F. Zamponi, Rev. Mod. Phys. **82**, 789 (2010).
[3] J. C. Dyre, Rev. Mod. Phys. **78**, 953 (2006).
[4] K. Binder and W. Kob, *Glassy Materials and Disordered Solids: An Introduction to Their Statistical Mechanics* (World Scientific, Singapore, 2011).
[5] W. Götze, *Complex Dynamics of Glass-Forming Liquids: A Mode-Coupling Theory* (Oxford University Press on Demand, New York, 2009), Vol. 143.
[6] C. Luo, J. F. Robinson, I. Pihlajamaa, V. E. Debets, C. P. Royall, and L. M. C. Janssen, Phys. Rev. Lett. **129**, 145501 (2022).
[7] T. Hecksher, A. I. Nielsen, N. B. Olsen, and J. C. Dyre, Nat. Phys. **4**, 737 (2008).
[8] G. Brambilla, D. El Masri, M. Pierno, L. Berthier, L. Cipelletti, G. Petekidis, and A. B. Schofield, Phys. Rev. Lett. **102**, 085703 (2009).
[9] H. Tanaka, T. Kawasaki, H. Shintani, and K. Watanabe, Nat. Mater. **9**, 324 (2010).
[10] S. Vivek, C. P. Kelleher, P. M. Chaikin, and E. R. Weeks, Proc. Natl. Acad. Sci. U.S.A. **114**, 1850 (2017).
[11] J. E. Hallett, F. Turci, and C. P. Royall, Nat. Commun. **9**, 3272 (2018).
[12] I. Tah, S. Sengupta, S. Sastry, C. Dasgupta, and S. Karmakar, Phys. Rev. Lett. **121**, 085703 (2018).
[13] W. Kob and L. Berthier, Phys. Rev. Lett. **110**, 245702 (2013).
[14] G. Biroli, S. Karmakar, and I. Procaccia, Phys. Rev. Lett. **111**, 165701 (2013).
[15] H. B. Yu, R. Richert, R. Maaß, and K. Samwer, Phys. Rev. Lett. **115**, 135701 (2015).
[16] A. Ninarello, L. Berthier, and D. Coslovich, Phys. Rev. X **7**, 021039 (2017).
[17] H. Tong and H. Tanaka, Phys. Rev. X **8**, 011041 (2018).
[18] L. Wang, N. Xu, W. H. Wang, and P. Guan, Phys. Rev. Lett. **120**, 125502 (2018).
[19] S. Marín-Aguilar, H. H. Wensink, G. Foffi, and F. Smallenburg, Phys. Rev. Lett. **124**, 208005 (2020).
[20] L. Berthier and D. R. Reichman, Nat. Rev. Phys. **5**, 102 (2023).
[21] C. P. Royall and S. R. Williams, Phys. Rep. **560**, 1 (2015).
[22] F. C. Frank, Proc. R. Soc. A **215**, 43 (1952).
[23] C. Xia, J. Li, Y. Cao, B. Kou, X. Xiao, K. Fezzaa, T. Xiao, and Y. Wang, Nat. Commun. **6**, 8409 (2015).
[24] G. M. Hocky, D. Coslovich, A. Ikeda, and D. R. Reichman, Phys. Rev. Lett. **113**, 157801 (2014).
[25] Z. Zheng, R. Ni, Y. Wang, and Y. Han, Sci. Adv. **7**, eabd1958 (2021).
[26] A. Widmer-Cooper, H. Perry, P. Harrowell, and D. R. Reichman, Nat. Phys. **4**, 711 (2008).
[27] S. S. Schoenholz, E. D. Cubuk, D. M. Sussman, E. Kaxiras, and A. J. Liu, Nat. Phys. **12**, 469 (2016).
[28] V. Bapst, T. Keck, A. Grabska-Barwińska, C. Donner, E. D. Cubuk, S. S. Schoenholz, A. Obika, A. W. Nelson, T. Back, D. Hassabis *et al.*, Nat. Phys. **16**, 448 (2020).
[29] H. Tong and H. Tanaka, Nat. Commun. **10**, 5596 (2019).
[30] D. Ma, A. D. Stoica, and X.-L. Wang, Nat. Mater. **8**, 30 (2009).
[31] Q. Zeng, Y. Lin, Y. Liu, Z. Zeng, C. Y. Shi, B. Zhang, H. Lou, S. V. Sinogeikin, Y. Kono, C. Kenney-Benson, C. Park, W. Yang, W. Wang, H. Sheng, H.-K. Mao, and W. L. Mao, Proc. Natl. Acad. Sci. U.S.A. **113**, 1714 (2016).

[32] Q. Zeng, Y. Kono, Y. Lin, Z. Zeng, J. Wang, S. V. Sinogeikin, C. Park, Y. Meng, W. Yang, H.-K. Mao, and W. L. Mao, Phys. Rev. Lett. **112**, 185502 (2014).

[33] D. Z. Chen, C. Y. Shi, Q. An, Q. Zeng, W. L. Mao, W. A. Goddard, and J. R. Greer, Science **349**, 1306 (2015).

[34] C. Xia, J. Li, B. Kou, Y. Cao, Z. Li, X. Xiao, Y. Fu, T. Xiao, L. Hong, J. Zhang *et al.*, Phys. Rev. Lett. **118**, 238002 (2017).

[35] H. Zhang, K. Qiao, and Y. Han, Nat. Commun. **11**, 2005 (2020).

[36] H. Zhang, C. Luo, Z. Zheng, and Y. Han, Acta Mater. **246**, 118700 (2023).

[37] J. D. Weeks, D. Chandler, and H. C. Andersen, J. Chem. Phys. **54**, 5237 (1971).

[38] C. Mayer, E. Zaccarelli, E. Stiakakis, C. Likos, F. Sciortino, A. Munam, M. Gauthier, N. Hadjichristidis, H. Iatrou, P. Tartaglia *et al.*, Nat. Mater. **7**, 780 (2008).

[39] E. R. Weeks, J. C. Crocker, A. C. Levitt, A. Schofield, and D. A. Weitz, Science **287**, 627 (2000).

[40] P. Chaudhuri, P. I. Hurtado, L. Berthier, and W. Kob, J. Chem. Phys. **142**, 174503 (2015).

[41] M. Laurati, P. Maßhoff, K. J. Mutch, S. U. Egelhaaf, and A. Zaccone, Phys. Rev. Lett. **118**, 018002 (2017).

[42] H.-B. Yu, M.-H. Yang, Y. Sun, F. Zhang, J.-B. Liu, C.-Z. Wang, K.-M. Ho, R. Richert, and K. Samwer, J. Phys. Chem. Lett. **9**, 5877 (2018).

[43] C. Rycroft, Chaos **19**, 041111 (2009).

[44] J. M. Rieser, C. P. Goodrich, A. J. Liu, and D. J. Durian, Phys. Rev. Lett. **116**, 088001 (2016).

[45] J. Yang, Y.-J. Wang, E. Ma, A. Zaccone, L. H. Dai, and M. Q. Jiang, Phys. Rev. Lett. **122**, 015501 (2019).

[46] S. Plimpton, J. Comput. Phys. **117**, 1 (1995).

[47] M. N. Bannerman, R. Sargant, and L. Lue, J. Comput. Chem. **32**, 3329 (2011).

[48] See Supplemental Material at http://link.aps.org/supplemental/10.1103/PhysRevLett.132.078201 for simulation details, which includes Refs. [49–61].

[49] F. H. Stillinger and B. D. Lubachevsky, J. Stat. Phys. **73**, 497 (1993).

[50] E. Bitzek, P. Koskinen, F. Gähler, M. Moseler, and P. Gumbsch, Phys. Rev. Lett. **97**, 170201 (2006).

[51] A. M. Alsayed, M. F. Islam, J. Zhang, P. J. Collings, and A. G. Yodh, Science **309**, 1207 (2005).

[52] G. L. Hunter and E. R. Weeks, Rep. Prog. Phys. **75**, 066501 (2012).

[53] J. C. Crocker and D. G. Grier, J. Colloid Interface Sci. **179**, 298 (1996).

[54] B. Li, D. Zhou, and Y. L. Han, Nat. Rev. Mater. **1**, 15011 (2016).

[55] J. Ding, M. Asta, and R. O. Ritchie, Proc. Natl. Acad. Sci. U.S.A. **114**, 8458 (2017).

[56] B. Li, K. Lou, W. Kob, and S. Granick, Nature (London) **587**, 225 (2020).

[57] H. Tong and H. Tanaka, Phys. Rev. Lett. **124**, 225501 (2020).

[58] C. Chang, H. P. Zhang, R. Zhao, F. C. Li, P. Luo, M. Z. Li, and H. Y. Bai, Nat. Mater. **21**, 1240 (2022).

[59] Y. Chen, Z. Ye, K. Wang, J. Huang, H. Tong, Y. Jin, K. Chen, H. Tanaka, and P. Tan, Nat. Phys. **19**, 969 (2023).

[60] M. Ozawa, A. Ikeda, K. Miyazaki, and W. Kob, Phys. Rev. Lett. **121**, 205501 (2018).

[61] C. Scalliet, L. Berthier, and F. Zamponi, Nat. Commun. **10**, 5102 (2019).

[62] G. E. Schröder-Turk, W. Mickel, M. Schröter, G. W. Delaney, M. Saadatfar, T. J. Senden, K. Mecke, and T. Aste, Europhys. Lett. **90**, 34001 (2010).

[63] B. Illing, S. Fritschi, H. Kaiser, C. L. Klix, G. Maret, and P. Keim, Proc. Natl. Acad. Sci. U.S.A. **114**, 1856 (2017).

[64] W. Li, Y. Peng, Y. Zhang, T. Still, A. Yodh, and Y. Han, Proc. Natl. Acad. Sci. U.S.A. **117**, 24055 (2020).

[65] Q. Zhang, W. Li, K. Qiao, and Y. Han, Sci. Adv. **9**, eadf1101 (2023).

[66] F. W. Starr, S. Sastry, J. F. Douglas, and S. C. Glotzer, Phys. Rev. Lett. **89**, 125501 (2002).

[67] X. Cao, H. Zhang, and Y. Han, Nat. Commun. **8**, 362 (2017).

[68] D. Turnbull and M. H. Cohen, J. Chem. Phys. **34**, 120 (1961).

[69] W. H. Wang, Prog. Mater. Sci. **57**, 487 (2012).

[70] S. Mazoyer, F. Ebert, G. Maret, and P. Keim, Europhys. Lett. **88**, 66004 (2010).

[71] M. L. Manning and A. J. Liu, Phys. Rev. Lett. **107**, 108302 (2011).

[72] E. D. Cubuk, S. S. Schoenholz, J. M. Rieser, B. D. Malone, J. Rottler, D. J. Durian, E. Kaxiras, and A. J. Liu, Phys. Rev. Lett. **114**, 108001 (2015).

[73] P. Schall, D. A. Weitz, and F. Spaepen, Science **318**, 1895 (2007).

[74] D. Richard, G. Kapteijns, J. A. Giannini, M. L. Manning, and E. Lerner, Phys. Rev. Lett. **126**, 015501 (2021).

[75] U. Gasser, E. R. Weeks, A. Schofield, P. Pusey, and D. Weitz, Science **292**, 258 (2001).

[76] E. Zaccarelli, C. Valeriani, E. Sanz, W. C. K. Poon, M. E. Cates, and P. N. Pusey, Phys. Rev. Lett. **103**, 135704 (2009).

[77] H. Zhang, S. Peng, X. Zhou, and X. Ju, Europhys. Lett. **107**, 46002 (2014).

[78] Q. Gao, J. Ai, S. Tang, M. Li, Y. Chen, J. Huang, H. Tong, L. Xu, L. Xu, H. Tanaka *et al.*, Nat. Mater. **20**, 1431 (2021).

[79] Z. Wang, F. Wang, Y. Peng, Z. Zheng, and Y. Han, Science **338**, 87 (2012).